Fusion Engineering and Design 199 (2024) 114102

Contents lists available at ScienceDirect

Fusion Engineering and Design

journal homepage: www.elsevier.com/locate/fusengdes

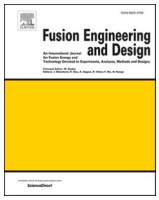

Characterization of liquid lithium corrosion for fusion reactor materials

Cody D. Moynihan [a], Steven Stemmley [a], Brady Moore [a], Riley Trendler [a], Md. Amzad Hossain [a,b,*], David N. Ruzic [a,*]

[a] Center for Plasma-Material Interactions, Department of Nuclear, Plasma, Radiological, and Engineering, University of Illinois at Urbana-Champaign, Urbana, IL 61801, USA

[b] Department of Electrical and Electronic Engineering, Jashore University of Science and Technology, Jashore 7408, Bangladesh

ARTICLE INFO

Keywords:
Liquid lithium
Corrosion
Characterization
Fusion material
Nuclear reactor
PFCs

ABSTRACT

As fusion devices push to become more compact, economical, and high performance, one potentially enabling technology is liquid lithium-based plasma-facing components (LL-PFCs). In our work, a new experimental setup was created to investigate the corrosion of seven fusion-relevant materials at 300 °C for 2000 h (≈3 months). A suite of surface, chemical, and imaging diagnostics were performed to determine the compatibility of the materials with liquid lithium. The seven materials were: tungsten, molybdenum, 304 stainless steel, 316 stainless steel, Inconel 625, silver-plated 316 stainless steel, and aluminum bronze. These materials can be roughly split into three categories: 1) refractory metals traditionally used as solid PFCs, 2) structural materials used for supports, and 3) bolt materials used for securing structures. Each material was submerged in a liquid-lithium filled canister and analyzed with a suite of chemical and imaging techniques. After investigation, it was determined that all the refractory and structural materials had a corrosion resistance of <1.0 μm/yr which will likely be an acceptable rate for future devices. However, both the silver-plated 316 stainless steel and aluminum bronze showed significant degradation over the course of the testing.

1. Introduction

The use of lithium as the plasma-facing surface for fusion can provide a myriad of benefits, including increased fusing volume, better fuel particle handling, and a reduction in damaging off-normal events [1]. Increasing the fusing volume enables more energy production per unit volume of reactor. Enhancing the fuel handling can lower the tritium inventory at the reactor site, making reactor licensing cheaper and quicker. A reduction in the frequency and amplitude of edge localized modes (ELMs) has been shown experimentally [2] which would mean less damage, maintenance, and down-time for a fusion pilot plant (FPP) / power station. However, the use of liquid lithium in these devices comes with a variety of challenges. The conductive fluid must be fully controlled in the system as it travels through spatially-varying magnetic fields. A full understanding of magnetohydrodynamics [3] and wetting dynamics [4] of the lithium in these systems is needed for fusion technology. The extraction of entrained fuel species from the liquid lithium is required for steady-state operation [5–6]. The high reactivity between lithium and water means that water cannot be used as a coolant, because of the dangers of loss of coolant accident (LOCA), leading to a more complicated/less efficient heat exchange system. All of these issues are being investigated and have potential solutions.

The primary requirement for the development of the divertor plasma-facing components (PFCs) is the ability to handle the large heat flux received from the leaking particles [7–15]. Most solid PFC designs are created to withstand a steady-state heat flux of 10MW/m^2 [16], which is the expected heat flux in ITER, the world's largest fusion device. These solid PFC materials are relatively easy to create and have no moving parts, making them easy to utilize in devices. Out of all the potential solid PFC materials, tungsten has the most desirable properties and is the most technologically developed material. In FPP/power station design studies in order to simultaneously achieve high fusion power and 10MW/m^2, the incident angle between the plasma and the solid PFC is typically ~2° [17]. Transient off normal events can cause melting of solid PFCs. Once tungsten solidifies, the solid PFC has a completely different shape, possibly interfering with plasma performance. Also, sputtered tungsten can enter the plasma, cooling it, and, ultimately, resulting in plasma collapse. One additional problem in tungsten divertors is the formation of tungsten fuzz during helium bombardment [13–15].

* Corresponding authors.
E-mail addresses: mdamzadh@illinois.edu (Md.A. Hossain), druzic@illinois.edu (D.N. Ruzic).

https://doi.org/10.1016/j.fusengdes.2023.114102
Received 31 October 2023; Received in revised form 1 December 2023; Accepted 7 December 2023
Available online 19 December 2023

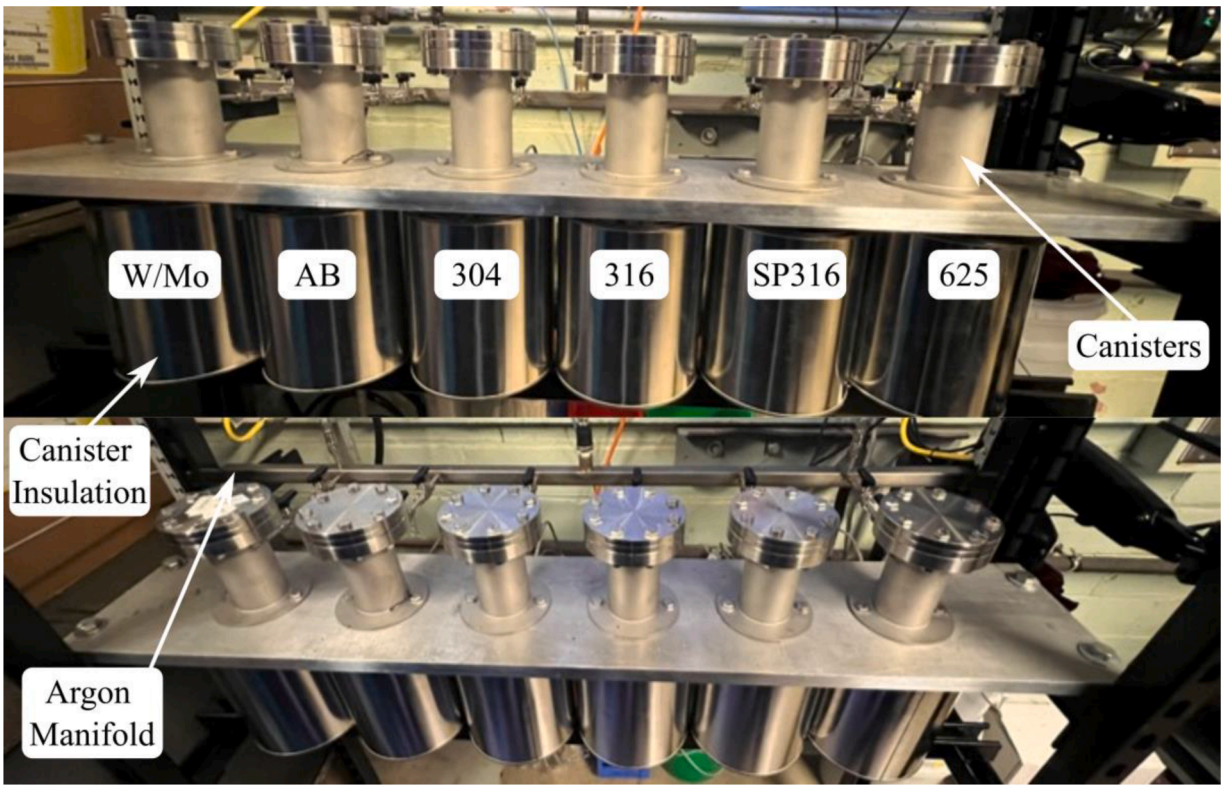

Fig. 1. Image showing the setup of the canisters holding the samples submerged in liquid lithium. The argon feed and canister insulation are also seen. Each canister is labelled with the corresponding material. Refer to Table 1 to compare the abbreviated names to full material names.

Table 1
Shortened names of each material, sometimes used for brevity.

Full Name	Shortened Name
Tungsten	W
Molybdenum	Mo
Aluminum Bronze	AB
304 Stainless Steel	304
316 Stainless Steel	316
Silver Plated 316 Stainless Steel	SP316
Inconel 625	625

In the case of lithium, it can only operate as a liquid divertor since lithium melts at 181 °C. A variety of different designs for liquid lithium divertors have been proposed. In terms of slow-flowing systems, the capillary porous system (CPS) [16] and the lithium vapor box [18] are being considered. In CPS, lithium is contained inside a porous mesh that allows the lithium to slowly move through the structures. The lithium vapor box utilizes lithium vapor to volumetrically absorb the diverted fusion power. Liquid-Metal Infused Trenches (LiMIT) [19] and Flowing Lithium Limiter (FLiLi) [20] utilize lithium flows of ~cm/s. LiMIT utilizes the heat flux from the plasma and thermoelectric magnetohydrodynamics (TEMHD) to drive the flow through millimeter sized structures. FLiLi relies on gravity driven flows down angled plates. Fast flow systems (>1 m/s) such as the International Fusion Material Irradiation Facility (IFMIF) [21] and Flowing Liquid Torus (FLIT) [22] have also been proposed. Both of these concepts utilized jets of lithium to absorb the heat flux from the plasma. Each of the above concepts utilizes the benefits of the liquid lithium surface to help handle the particle and heat flux in the fusion divertor. However, each of these concepts has to overcome the challenges of implementing a liquid lithium-based PFCs in IFMIF [23–24].

The vapor pressure of lithium is considerably higher than that of solid materials or other liquid metal candidates [23]. A variety of techniques are being investigated to tackle the real-time removal of hydrogen isotopes from liquid lithium [24–25]. Modeling of lithium flows in a variety of magnetic configuration is ongoing in many national labs and universities [26–27]. Additionally, the free surface stability needs to be understood to avoid exposure of underlying structures to the plasma or production of large droplets that can enter the plasma. Both modeling and experimental work have been performed to predict and reduce surface instabilities [27–28]. To investigate the severe corrosion of materials under lithium exposure, many studies have been performed analyzing lithium corrosion dynamics of metals, mostly for the nuclear fusion sector [28–33]. Substantial previous work has been performed in an attempt to gain the understanding to develop materials that are not corroded by liquid lithium in fusion devices [34–40]. In order for lithium to be utilized in a nuclear fusion device, it must be compatible with all the materials it comes into contact with. Numerous studies conducted on lithium corrosion, very few are conducted at the operating temperatures expected in a lithium divertor (≈300 °C). A continued work is needed to investigate the compatibility of desired materials in the fusion-relevant lithium environment.

This work studies the alkaline nature of lithium which makes it highly corrosive to a wide array of materials. The objectives of this work were to investigate liquid lithium corrosion in nuclear fusion reactor materials and to characterize our samples using various diagnostic tools. In Section 2, the experimental design and operation details were explained in detail. The findings on seven materials: tungsten, molybdenum, 304 stainless steel, 316 stainless steel, Inconel 625, silver-plated 316 stainless steel, and aluminum bronze were discussed in Section 3. Finally, in Section 4, the results obtained in this work were summarized.

2. Experimental setup

To test the corrosion of materials in liquid lithium for extended periods of time, a new system needed to be developed. This new system was designed to test six materials at a same time in static liquid lithium

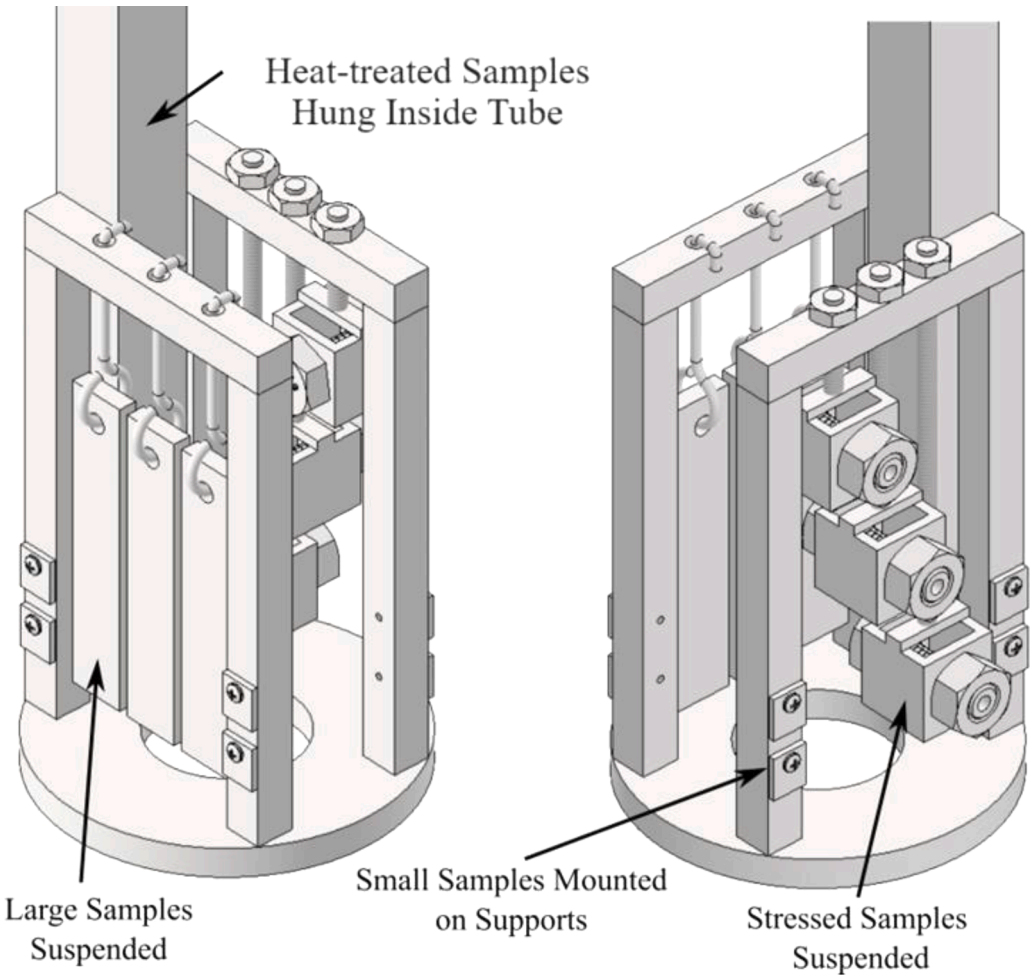

Fig. 2. CAD of the sample stand highlighting how each sample type is mounted inside the canister. Left is for large samples and Right is for bolts which much maintain integrity even under stress.

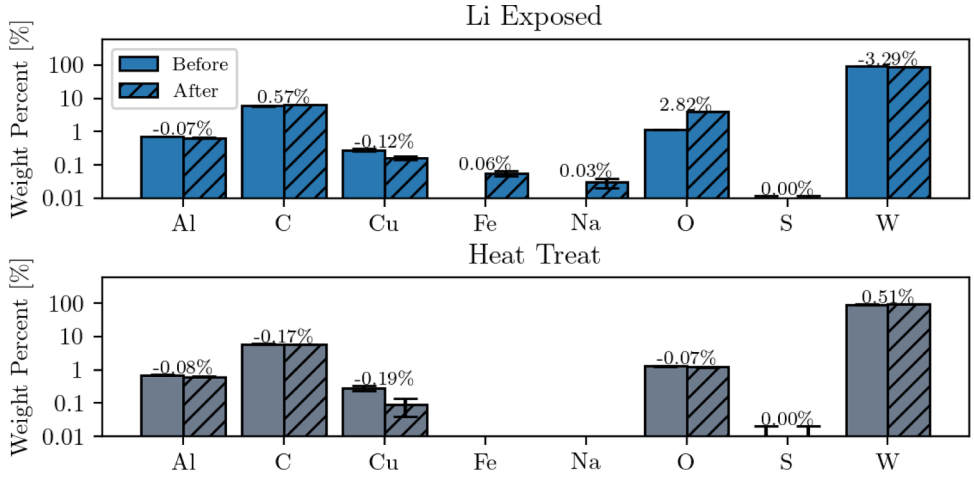

Fig. 3a. EDS of the tungsten sample, showing average surface composition, obtained from EDS analysis at 500X magnification for lithium-exposed samples (blue) and heat-treated sample (gray). Some pickup of Fe is evident and is expected to have come from the stainless-steel vessel. Oxygen has increased on the surface, likely due to the formation of lithium-oxide. The tungsten concentration has gone down with the increase in these other elements. Error bars represent the standard deviation in composition and the numbers above the bars give the change in average composition after testing.

Table 2
Mass measurements and corrosion rate for the large tungsten samples. A consistent amount of mass was lost in all three of the large samples. For the detectable mass change, a green check mark (✓) suggests that the mass loss was outside of the error bars, while a red (X) suggests otherwise.

Sample	Mass Before (g)	Mass After (g)	Mass Change (g)	Detectable Mass Change	Corrosion Rate (μmyr^{-1})
L1	25.281 ± 0.0003	25.276 ± 0.0005	−0.005 ± 0.0006	✓	−0.88 ± 0.103
L2	26.294 ± 0.0005	26.290 ± 0.0005	−0.004 ± 0.0007	✓	−0.70 ± 0.123
L3	25.692 ± 0.0008	25.687 ± 0.0009	−0.005 ± 0.0012	✓	−0.88 ± 0.211
Average	–	–	−0.005 ± 0.0005	✓	−0.82 ± 0.088

Table 3
Mass measurements and corrosion rate for the large molybdenum samples. Mass was lost in each of the large samples, however, the mass loss was less than tungsten. Using the corrosion rate to remove the density dependence reveals that the corrosion is slightly slower for molybdenum than tungsten. For the detectable mass change, a green check mark (✓) suggests that the mass loss was outside of the error bars, while a red (X) suggests otherwise.

Sample	Mass Before (g)	Mass After (g)	Mass Change (g)	Detectable Mass Change	Corrosion Rate (μmyr^{-1})
L1	13.287 ± 0.0005	13.286 ± 0.0003	−0.001 ± 0.0006	✓	−0.33 ± 0.194
L2	13.340 ± 0.0008	13.337 ± 0.0005	−0.003 ± 0.0009	✓	−0.99 ± 0.312
L3	13.406 ± 0.0005	13.403 ± 0.0005	−0.003 ± 0.0007	✓	−0.99 ± 0.234
Average	–	–	−0.002 ± 0.0004	✓	−0.77 ± 0.145

at 300 °C for 2000 h. These particular design choices were made to simulate the operational temperature of future lithium-based reactors. 300 °C is a good choice for operating temperature because it is above the melting temperature of the lithium, while keeping the vapor pressure low ($<10^{-6}$ Torr) [31]. Moreover, the vapor pressure of lithium becomes quite high beyond 450 °C. For this reason, many liquid lithium divertor component designs attempt to have an operational temperature near 300 °C. The duration of 2000 h was chosen as it gives sufficient time for corrosion to occur while being reasonably achievable as a short-term experiment. The seven materials chosen to study where: tungsten, molybdenum, 304 stainless steel, 316 stainless steel, Inconel 625, aluminum bronze, and silver-plated 316 stainless steel. Each of these materials will potentially play a crucial role in future fusion reactors with liquid lithium-based PFCs, so their corrosion dynamics need to be understood under expected operating conditions.

Fig. 1 shows an image of the assembled canister mounted into the system. The buckets seen below the aluminum support are filled with fiberglass insulation to prevent excess heating of the surroundings and limit the amount of power required to keep the lithium at 300 °C. Table 1 gives a list of the abbreviated names used in Fig. 1 and sometimes used in the subsequent sections for brevity. A 316 stainless steel sample stand was placed inside each canister to hold and organize the samples during the experiment. Fig. 2 shows how samples were mounted onto the sample stand. For all but the molybdenum and tungsten canister, each of the three samples types were mounted into the sample stand. Small samples were screwed into the support structure and therefore were only exposed to lithium on five sides. Large samples were hung from the support structure by 316 stainless steel wire and saw full exposure to lithium. Stressed bolt samples were mounted inside a holder which was hung from the sample stand. Each stressed sample should have allowed lithium around the outside and inside of the bolt. The sample stand also allows for small samples suspended on a wire to be inserted into an isolated tube during the experiment. This allowed for these samples to experience the heating but not the lithium exposure during the 2000 h, allowing for lithium corrosion versus thermal treatment effects to be distinguished.

A safe and fully controllable operation was desired, with all the data acquisition and system control computerized. As such, custom printed circuit boards were made for control and measurement of the heater output. A LabJack data acquisition device was used to collect the analog

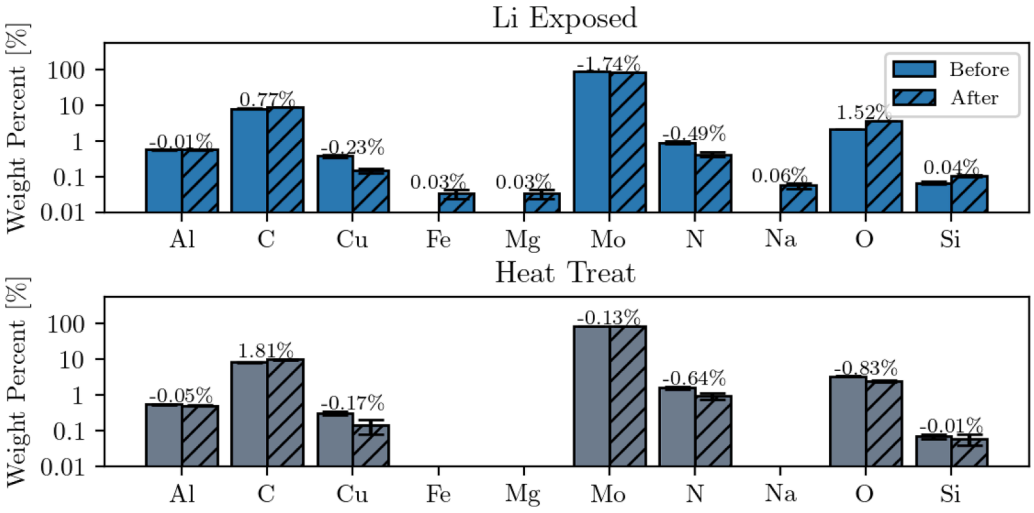

Fig. 3b. EDS of the molybdenum sample, showing average quantitative surface composition obtained from EDS analysis at 10000X magnification for all lithium-exposed samples (blue) and heat-treated sample (gray). Like the tungsten, the molybdenum seemed to pick up stainless-steel components from the canister. Oxygen is also present on the surface after lithium exposure, with a slight decrease in molybdenum. Error bars represent the standard deviation in composition and the numbers above the bars give the change in average composition after testing.

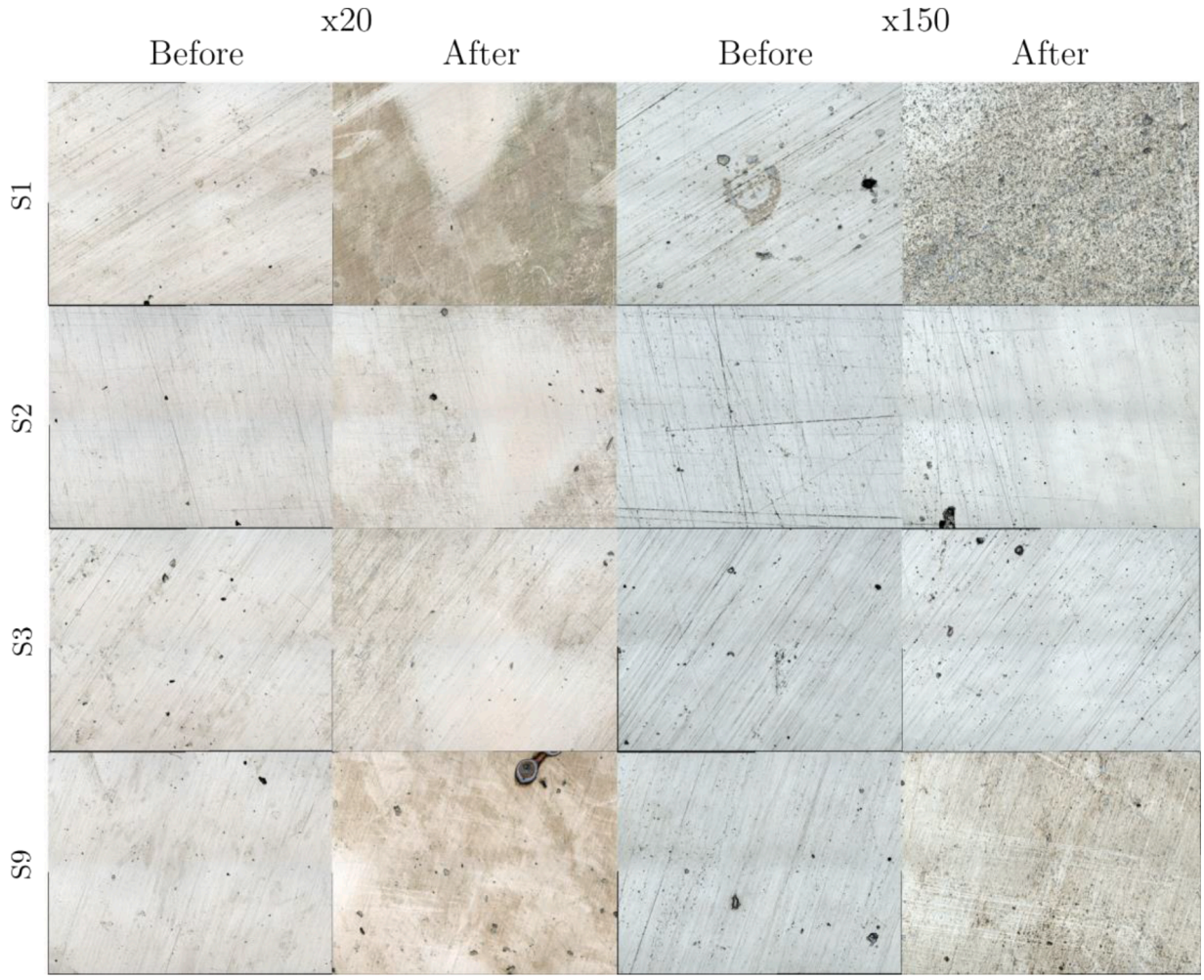

Fig. 4a. 304 stainless steel sample, combined laser and optical images obtained by 3D profilometry before and after testing.

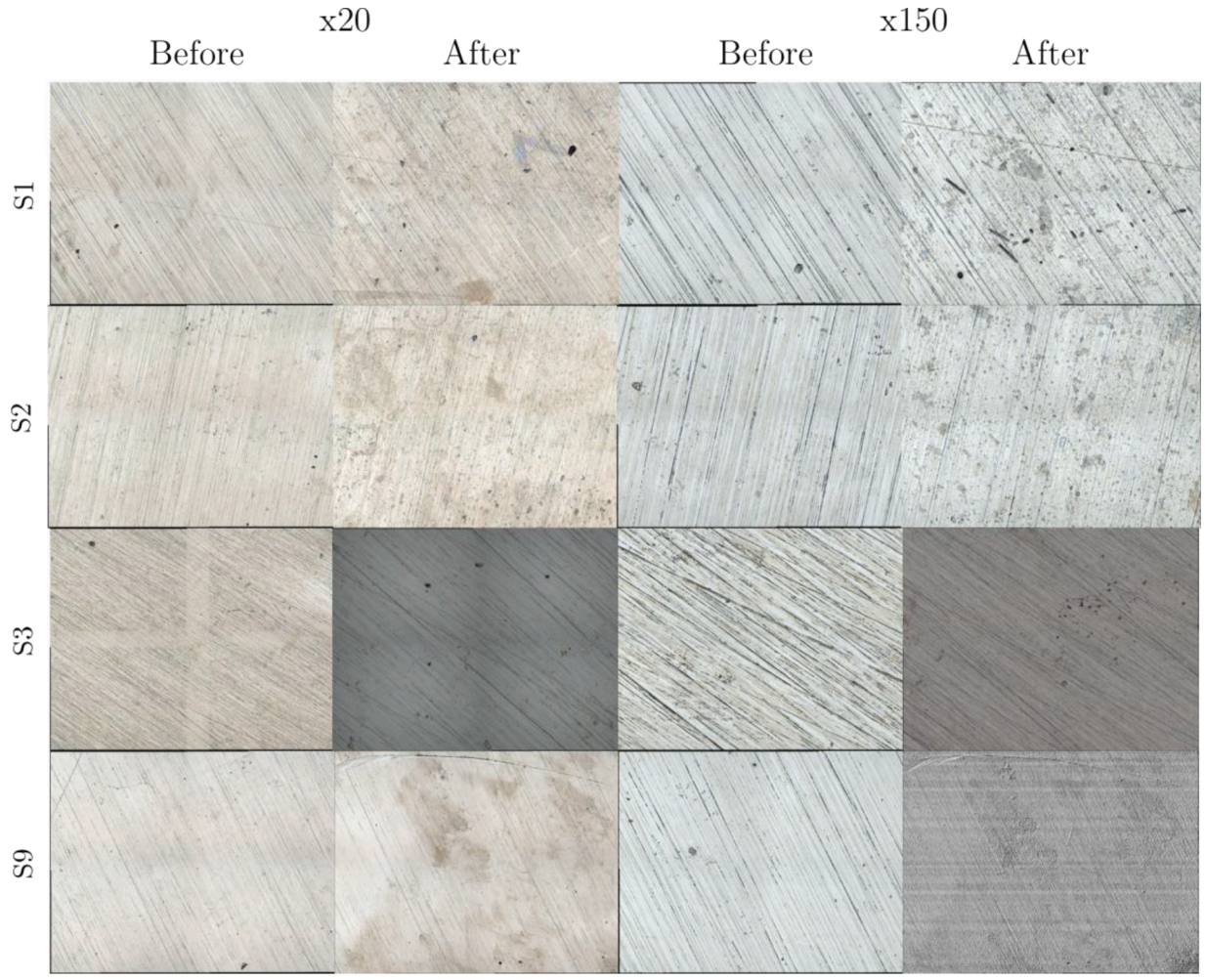

Fig. 4b. 316 stainless steel sample (small sample), combined laser and optical images obtained by 3D profilometry before and after testing.

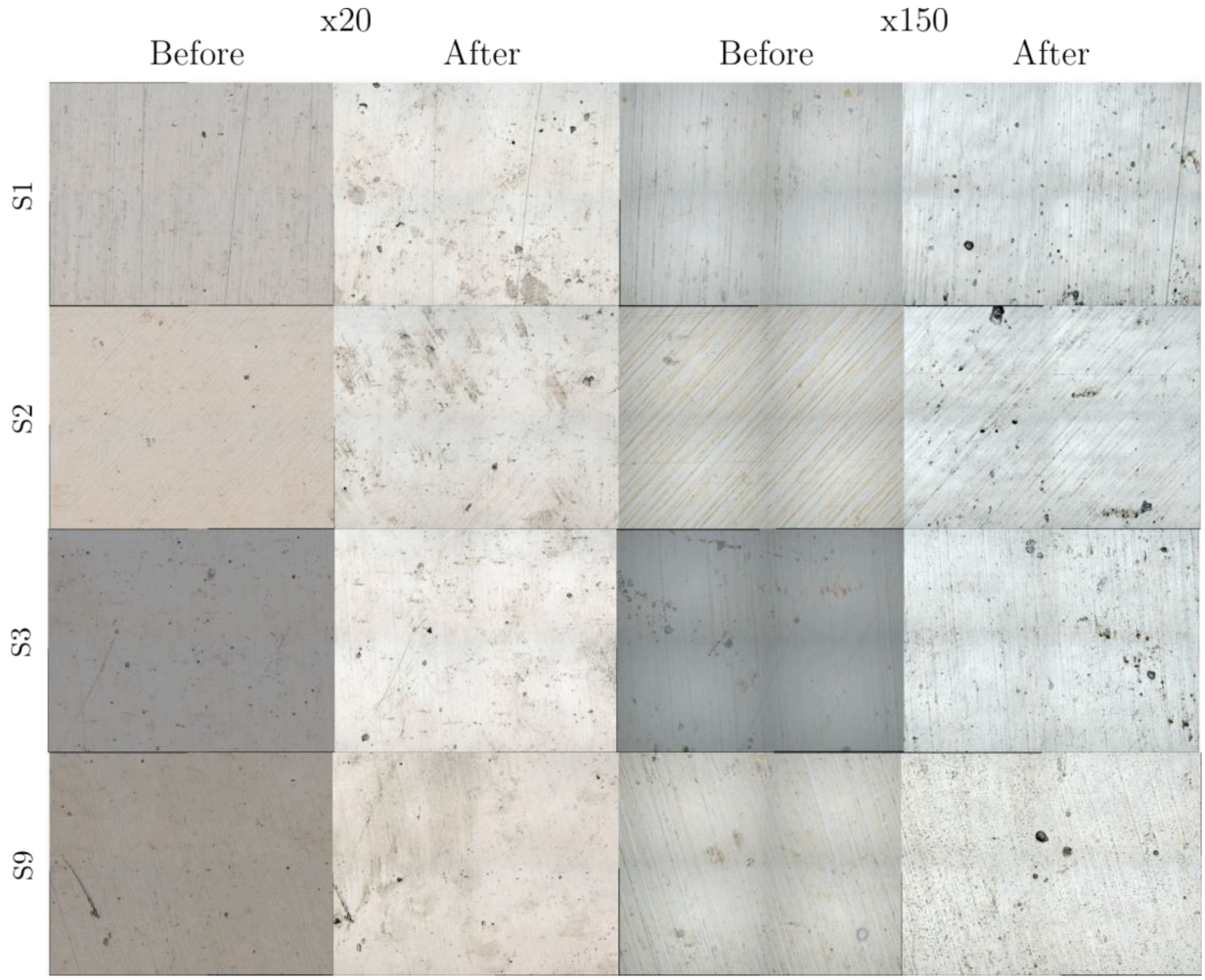

Fig. 4c. Inconel 625, combined laser and optical images obtained by 3D profilometry before and after testing.

signals and control the digital communication sent to other electronics. The Labjack was able to control the heater output and read the six thermocouples, six heater currents, and system pressure. A Python software was written to allow the user to control the experiment and save the required data. Each of the six canisters were controlled individually, meaning that the 2000 h of one material did not have to overlap with that of another canister.

Along with data saving and system control, the software was built to include error tracking that could respond to off-normal events that required system maintenance, such as over-heating or heater failure. In the event of an error, the system would respond to the problem and send users an alert email to describe the problem with the system. Users could then remotely log into the system and check on system status or perform additional system control steps. Along with alert emails, the system would send daily update emails to the users to ensure that everything was working properly. It was this software and control system that allowed for the safe overnight and extended operation of this liquid lithium system. The lithium we used had a purchased purity of 99.9%. The argon glovebox was handled to maintain a <0.1 ppm of both oxygen and water, and it is always kept at a positive pressure. Some nitrogen contamination is possible in the glovebox over time, but it was minimized as best as possible. Positive argon gas pressure and the double ball valve method during canister deployment throughout experiments was used to maintain the purity of lithium.

3. Results

3.1. Surface composition analysis of refractory materials

Refractory metals are traditionally used as solid PFCs. However, new liquid lithium PFC designs sometimes utilize the refractory metal as the substrate on which the lithium flows. This is done to ensure that significant material degradation does not occur if some of the underlying substrate is exposed to the plasma. Tungsten samples were placed inside the same canister as the molybdenum samples. This was due to the fact that refractory metals are not expected to be used as structural materials and no tensioned samples were tested. Since the canister sample stand was split between two materials, four small samples were exposed to lithium, and two samples were heat-treated. Three large tungsten samples were loaded as well, the same as all other canisters. As with the tungsten samples, seven molybdenum samples (3 large, 4 small) samples were exposed to lithium, and two samples were only heat-treated. During the cleaning process, the molybdenum samples were handled the same properties as the tungsten samples.

Quantitative energy dispersive spectroscopy (EDS) data for the tungsten sample is shown in Fig. 3 (a). Negligible changes in composition are seen in the heat treat sample, and are most likely due to the EDS images being taken at different locations before/after heating. In the lithium exposed samples, the increases in iron, sodium, and oxygen are

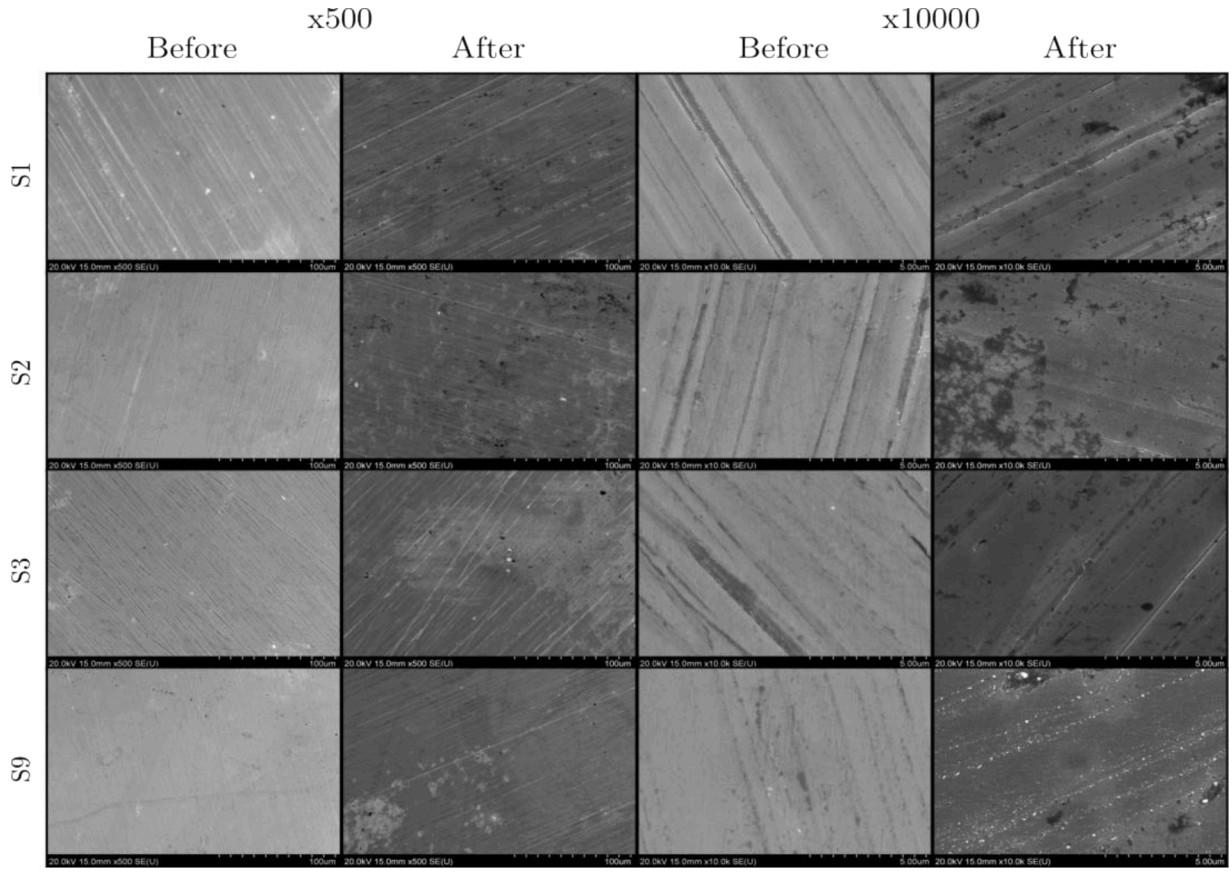

Fig. 4d. SEM images of 316 stainless-steel, before and after testing.

clearly seen. The loss in tungsten weight percent is a result of EDS enforcing the sum of all analyzed elements to be 100 wt%. Along with surface studies, bulk analysis methods were employed. Mass measurements of the large samples, along with detailed measurements, yield corrosion rates shown in Table 2. The samples clearly lost mass over the course of the 2000 hour test, yielding an average corrosion rate of $(0.820 \pm 0.088)\ \mu m \cdot yr^{-1}$.

Table 3 shows the mass loss of the large molybdenum samples. Minimal mass loss occurred over the 2000 h, corresponding to a corrosion rate of (0.770 ± 0.145) μm/yr. Fig. 3 (b) shows that a small pickup of iron was present on the surface, similar to the tungsten. In addition, oxygen increased on the surface.

3.2. Surface and composition analysis of structural materials

Structural materials are needed to create support structures, as well as the vacuum vessels needed for fusion systems. These same materials will often also be used as the tubing material for transporting lithium from an external reservoir into the reactor. Of particular interest, is the 300 series of stainless steels, which are often used by manufacturers for vacuum vessel fabrication. These alloys contain a mixture of elements, so understanding their corrosion is easiest done through experimentation with the exact alloy used. In some instances, advanced alloys with superior performance are required. One such alloy is Inconel 625, which is analyzed here with 304 stainless steel samples and 316 stainless steel samples. Fig. 4 (a)–(c) displays the profilometry images for the small 304 stainless steel, 316 stainless steel, and Inconel 625 samples, respectively.

SEM images as shown in Fig. 4 (d) does show some deposits on the surface of the sample after exposure for the 316 stainless-steel. Interestingly, the deposits on the heat-treated sample (S9) seem to be a different material, as they have different contrast compared to the features on the lithium-exposed samples. SEM imaging in Fig. 4 (e) shows the same dark deposits as were present in the 316 stainless steel imaging.

3.3. Surface and composition analysis of bolt materials under stress

While bolts can be made from the same materials as used for structural components, those materials tend to suffer from galling, especially with thermal cycling. To combat this, materials are used that tend to provide some lubricity. Two common materials used in vacuum systems are silver-plated 316 stainless steel and aluminum bronze. The silver-plating acts as a protective layer on the stainless steel and prevents the galling that commonly happens. Aluminum bronze is used for its high tensile strength and corrosion resistance in acidic and humid environments.

Fig. 9 shows the samples after cleaning and just prior to baking. Aluminum bronze was severely attacked by liquid lithium at 300 °C. Upon initial inspection, the lithium looked like all other canisters after cooling shown in Fig. 9(a), but upon placement in the cleaning water, particulates rapidly appeared in the water shown in Fig. 9(b). Once the canister was removed from the cleaning water, lithium reaction products filled nearly up to the top of the sample stand shown in Fig. 9(d). After the stand was removed from the canister, these products could be seen clinging to the samples and stand shown in Fig. 9(g). These reaction products were rinsed off the sample stand shown in Fig. 9(e) and a thinner layer of the products still remained.

After this bulk water cleaning, the water was still clear with many particulates floating around, both on the surface and in solution. The samples were removed from the sample stand and the cleaning with distilled water and acetone began. During the removal, all of the bolts

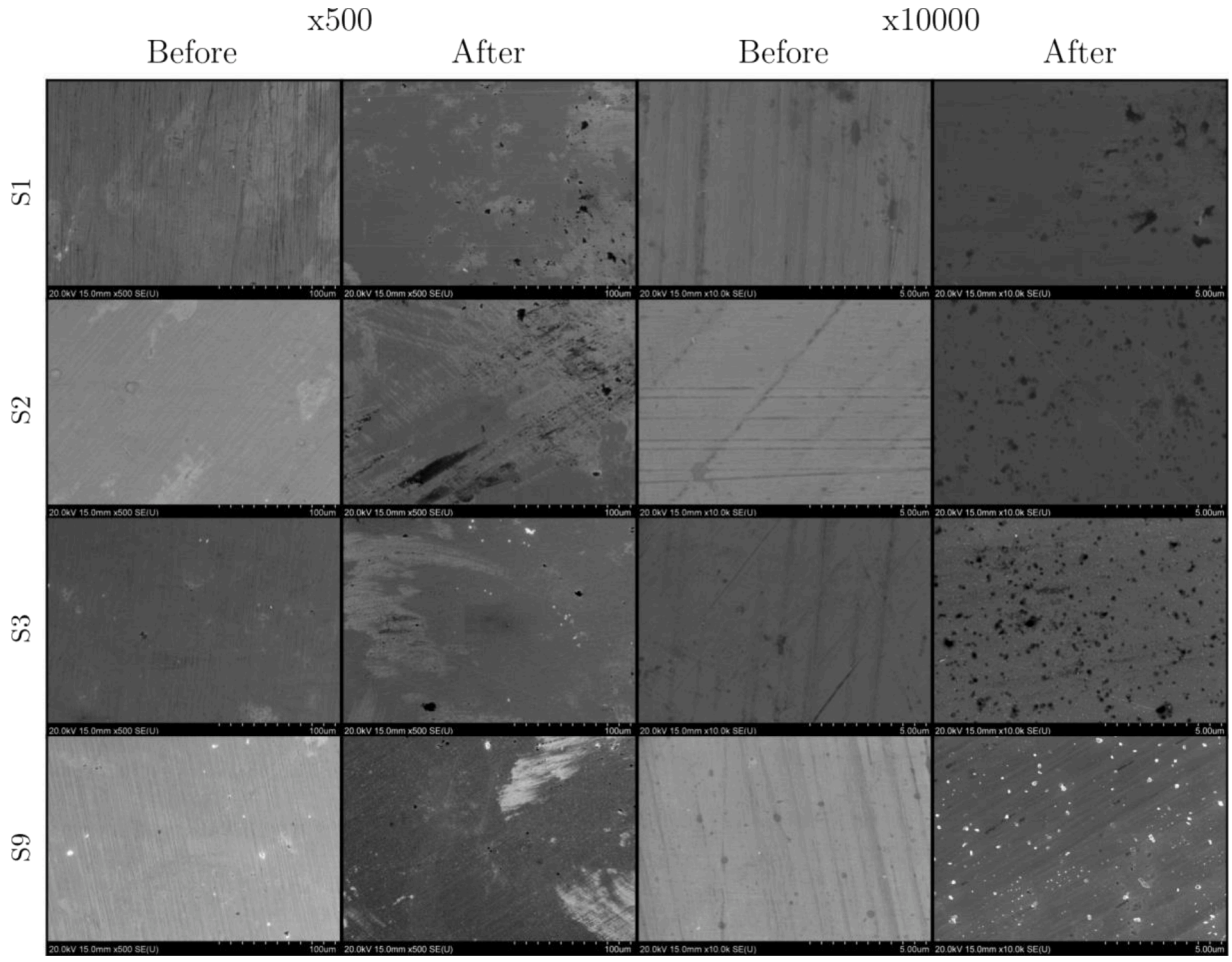

Fig. 4e. SEM images of the Inconel 625 before and after testing.

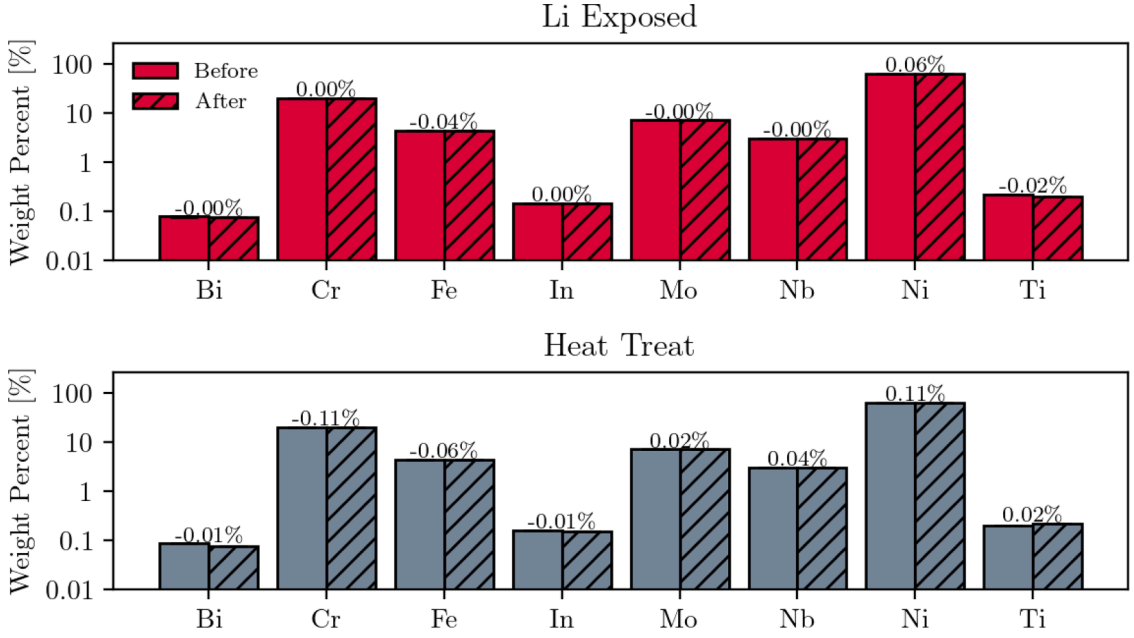

Fig. 5. XRF chemical compositions before and after lithium exposure. Like the EDS results, the XRF scans show no change in the composition of the Inconel samples. In this case, the heat-treated sample actually have more variation than the lithium exposed samples. The height of the bars represents the average composition of samples S1-S3. The text above the bars represents the change in chemical composition after lithium exposure.

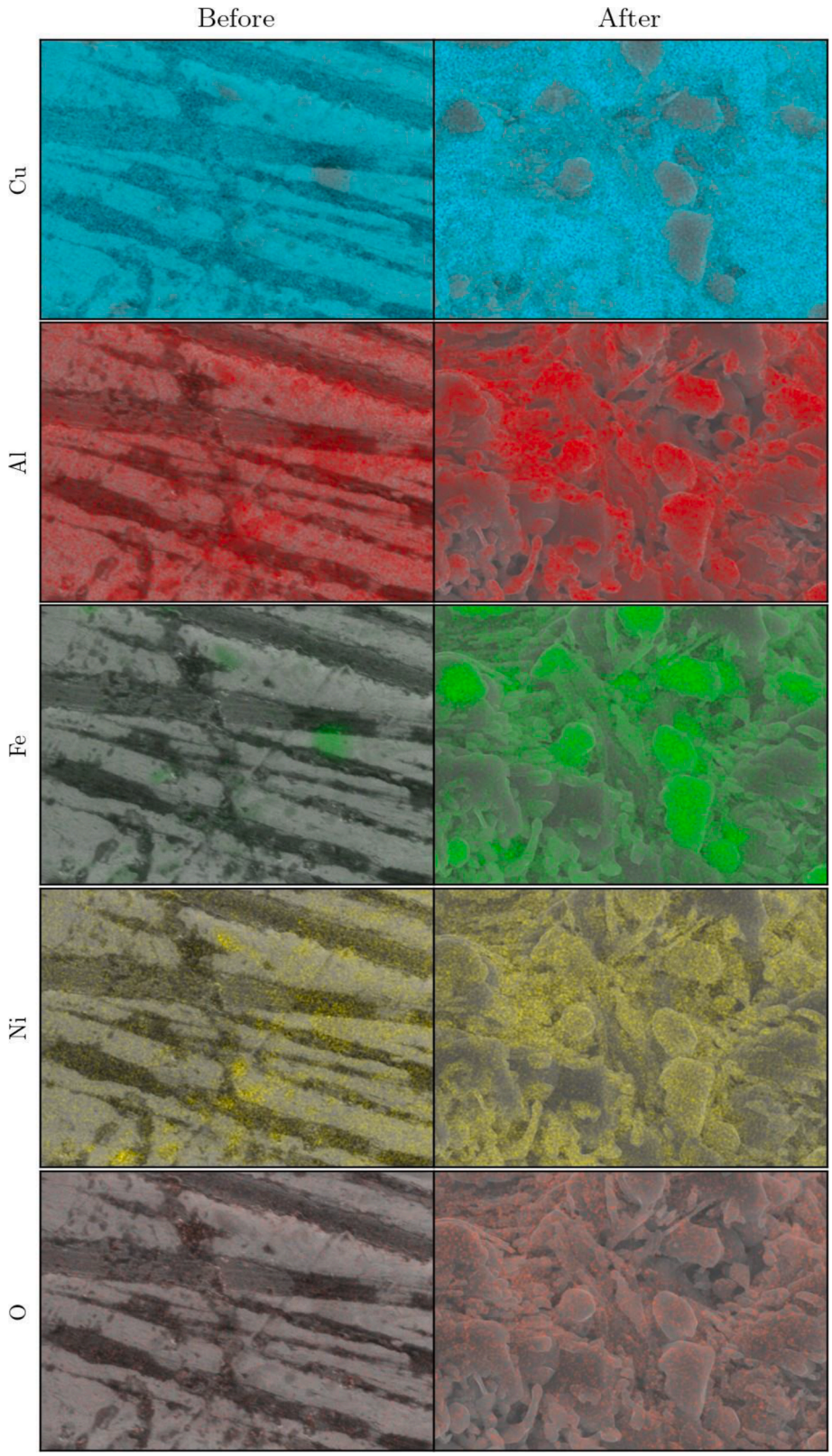

Fig. 6. EDS surface composition images of a representative lithium-exposed small aluminum bronze sample. Copper is depleted in regions with heightened Fe concentrations. Ni-Al compounds seem to form in the surface, similar to the silver-plated 316 stainless steel. Oxygen present on the surface is most likely signifying the formation of lithium-oxide in the surface.

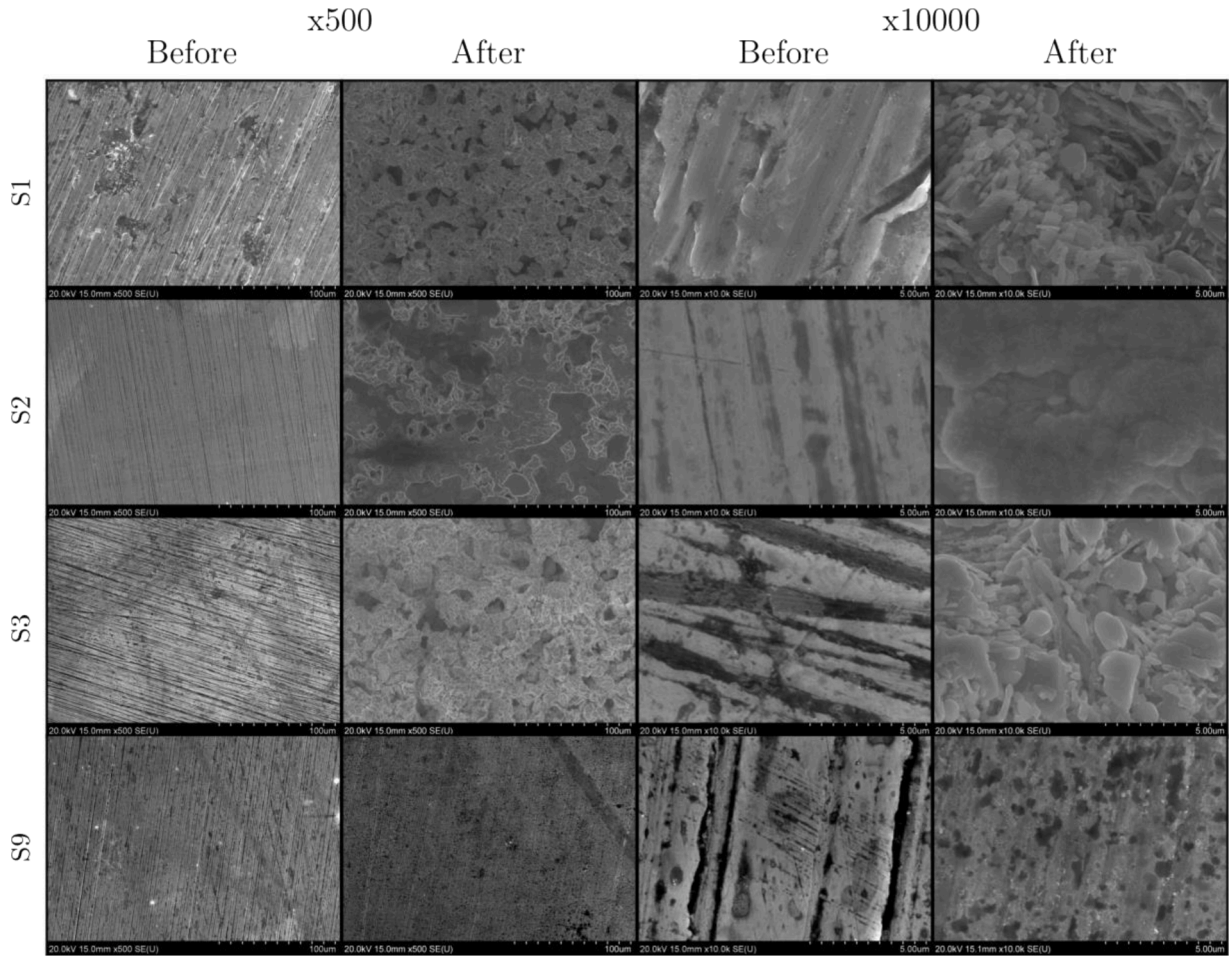

Fig. 7. SEM images before and after testing for the aluminum bronze. The left two columns are at a x500 magnification and the right two at a x10000 magnification. The porosity of the sample is easily seen in the SEM images after lithium exposure. However, chemical analysis is needed to understand the compounds in each region of the porous media. Samples S1-S3 were exposed to lithium and sample S9 was only heat-treated.

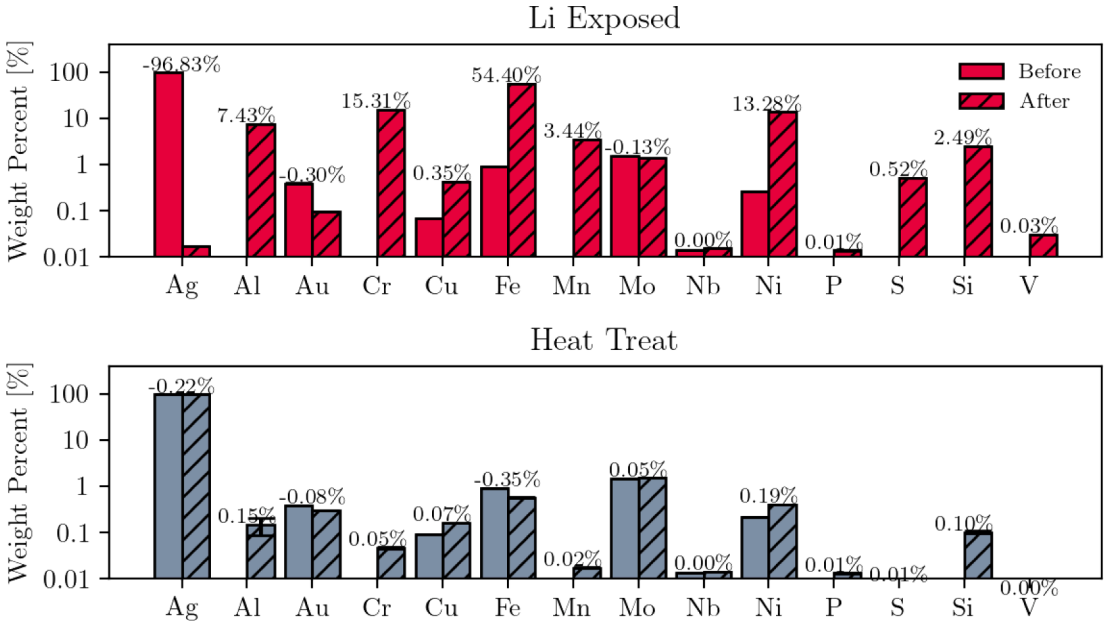

Fig. 8. XRF chemical compositions before and after lithium exposure. Like the other analyses, XRF confirms the nearly complete removal of the silver plating. Again, the composition changes to that of the underlying 316 stainless steel. The height of the bars represents the average composition of samples S1-S3. The text above the bars represents the change in chemical composition after lithium exposure.

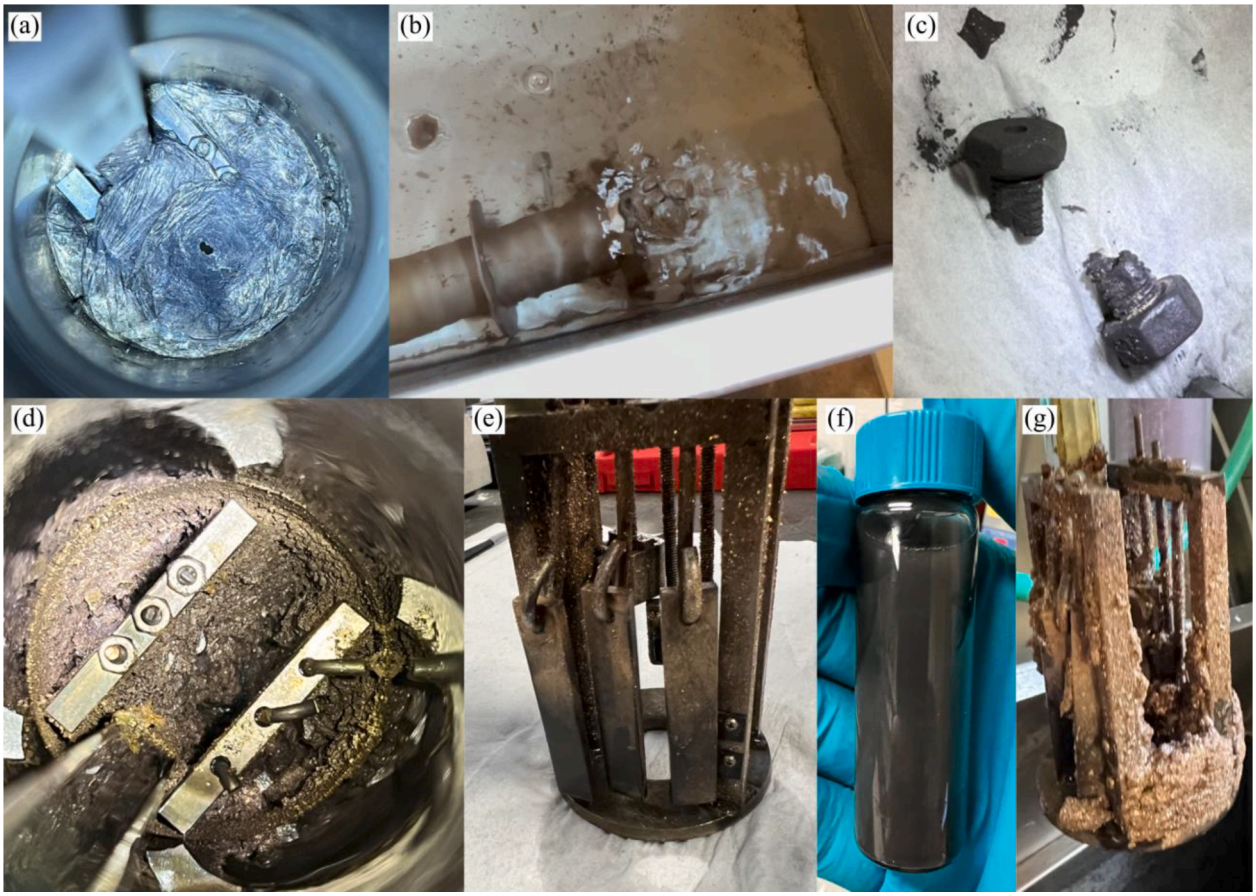

Fig. 9. Images of the cleaning process for the aluminum bronze samples. (a) Slag formed on the top of the lithium after removing from the experiment and exposing to air. (b) Reaction of lithium in canister with the cleaning water. Particulates are seen flowing from the canister immediately. (c) Bolt sample broken into two pieces after removal. (d) Corrosion products left in the canister after water cleaning. These products were granular and the sample stand could be removed. (e) Sample stand was covered with corrosion products after water cleaning. These products could not be simply washed or wiped from the surface. (f) Black discolored water during individual sample cleaning and sonication. (g) Image of the sample stand as it was removed from the canister. Corrosion products covered the entire stand.

completely snapped shown in Fig. 9(c) and the nuts could not be removed. The water turned black under sonication with distilled water shown in Fig. 9(f) and took multiple rounds of sonication to run clear.

4. Discussion

For refractory metals, the obtained corrosion rate ((0.820 ± 0.088) $\mu m \cdot yr^{-1}$) is likely acceptable in most situations, as PFCs lifetimes are typically less than five years resulting in sub-5 μm surface loss. For structural metals, only mild surface discoloration is seen on all the samples, including the heat-treated sample [see Fig. 4 (a)]. It seems that the heating may have caused the discoloration rather than the lithium exposure. The left two columns show results at 20X magnification and the right two columns 150X magnification. Sample S9 was not exposed to lithium and only thermally treated as shown in Fig. 4 (a). Very little change is seen in the surface apart from some large number of particulates [see Fig. 4 (b)]. It is possible that these particulates are corrosion products or simply dust on the sample after cleaning. The left two columns show results at 20X magnification and the right two columns 150X magnification. Sample S9 was not exposed to lithium and only thermally treated as shown in Fig. 4 (b). The Inconel 625 shows very little surface degradation under optical profilometry, performing better than both stainless steels [see Fig. 4 (c)]. Like the 316 stainless steel, the surface has some larger particulates present after exposure. The left two columns show results at 20X magnification and the right two columns 150X magnification. Sample S9 was not exposed to lithium and only thermally treated as shown in Fig. 4 (c). On average, little discoloration is observed in the post-Li samples compared to the pre-Li images. Optical profilometry of the 316 stainless steel shows very minimal surface discoloration or tarnishing as shown in Fig. 4 (b). No major surface changes are apparent from the images. Inconel 625 did not show the same surface discoloration during 3D profilometry as the stainless steels as shown in Fig. 4 (c). However, there is significantly more dust or deposits on the surface after cleaning.

The surface looks very similar after lithium exposure at 500X, but some dark splotches seem to appear at higher magnification [see Fig. 4 (d)]. The composition of the material on the lithium-exposed versus heat-treated sample seem to be different based on the different contrast in the image. The left two columns are at a x500 magnification and the right two at a x10000 magnification. Samples S1-S3 were exposed to lithium and sample S9 was only heat treated as shown in Fig. 4 (d). In Inconel 625, Like the 316 stainless steel, dark splotches are present in the lithium exposed samples [see Fig. 4 (e)]. The depositions on the heat-treated sample appear to be a different material, as the contrast is significantly different. It is unclear if the splotches are raised off the surface of the samples. The left two columns are at a x500 magnification and the right two at a x10000 magnification. Samples S1-S3 were exposed to lithium and sample S9 was only heat treated as shown in Fig. 4 (e).

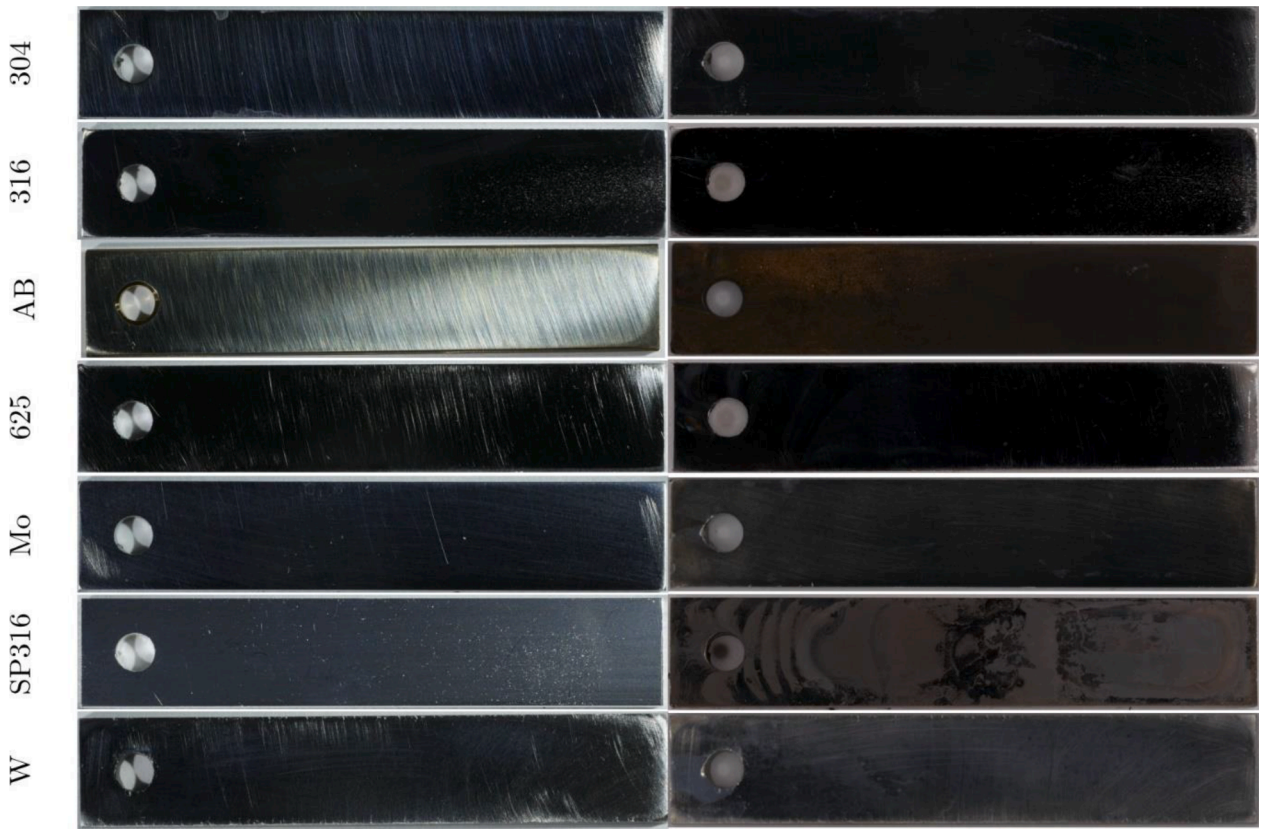

Fig. 10. Sample images of one large sample for each material tested before (left) and after (right) lithium exposure. Most materials are relatively unaffected by lithium exposure. The structural materials show no change in their surface appearance. The refractory metals show some discoloration and appear less reflective. The bolt materials (aluminum-bronze and silver-plated 316 stainless steel) are attacked extensively by the lithium.

Like EDS, XRF shows very high consistency between lithium exposed and heat-treated samples (see Fig. 5). Elemental imaging (shown in Fig. 6) show erosion / deposition of O, Ni, Fe, Al and Cu. It was observed that Ni-Al compounds seem to form in the surface. It also seems the copper depleted regions are filled with iron. Some small iron clusters were seen prior to exposure, so it is possible that the lithium simply removed all the surrounding material. In Fig. 7, SEM images reveal the porous nature of the samples after exposure. Lithium seemingly attacked the sample along grain boundaries to work its way into the surface. EDS shows that the surface is slightly depleted in copper, with an enrichment in Fe, Ni, and O. The oxygen is likely accompanied by lithium in the form of lithium-oxide. Overall, the sample seems to have a similar composition, with large pieces of material removed. XRF again confirms the removal of the silver plating, as seen in Fig. 8. Similarly, the components of the 316 stainless-steel appear in the analysis. As shown in Fig. 9, for bolt materials under stress, clearly, aluminum bronze cannot withstand lithium exposure. It seems that the reaction was ultimately limited by the availability of lithium to form reaction products or the solubility of elements into the lithium.

Fig. 10 shows images of the large samples before and after lithium exposure. Fig. 11 shows the corrosion rate comparison across materials. Table 4 gives qualitative results of each material. The refractory metals, tungsten and molybdenum, performed well in the lithium environment. Neither material suffered large mass loss during testing. In agreement with literature, the refractory metal corrosion seems to be based on the dissolution of the metal into the lithium solution. The structural materials, 304 stainless steel, 316 stainless steel, and Inconel 625, also performed well during the lithium exposure. Mass loss was minimal and the surfaces remained polished after exposure. Both of these groups of materials seem to be acceptable candidate materials for use in liquid lithium PFC environments. On the other hand, the bolt materials, silver-plated 316 stainless steel and aluminum bronze, completely failed under lithium exposure. The silver plating was entirely removed from the plated sample, nullifying the benefits of the coating and adding impurities to the lithium. Importantly, we believe that all of the lithium had reached with the aluminum bronze and if we had replenished the lithium, then all of the aluminum bronze would have reacted.

5. Conclusions

Liquid lithium-based PFCs offer a variety of benefits to fusion performance but come with a number of challenges, including flow control, reactivity, and corrosion. While primarily examining a nuclear fusion context, this study measured corrosion in lithium systems. Such measurements can become complicated because there are many factors that contribute to the corrosion dynamics. In order to understand how a material reacts with LL-PFCs, a comprehensive chemical analysis, surface analysis, and variety of imaging techniques were used.

A new experimental setup was designed and fabricated to test these seven materials. Operation at 300 °C for 2000 h was achieved through band heaters and the use of an automated data collection and control system. Safe overnight operation occurred by means of software with built-in safety protocols that could respond to off-normal events. Individual canisters were isolated from each other by means of a double ball valve system and software isolation that allowed individual canister control and timing. Lithium purity was maintained by positive argon pressure during experimentation and by the double ball valve system during canister placement. Materials were separated with the use of six individual canisters. Analysis was simplified by utilizing multiple sample shapes and sizes for the various analysis techniques.

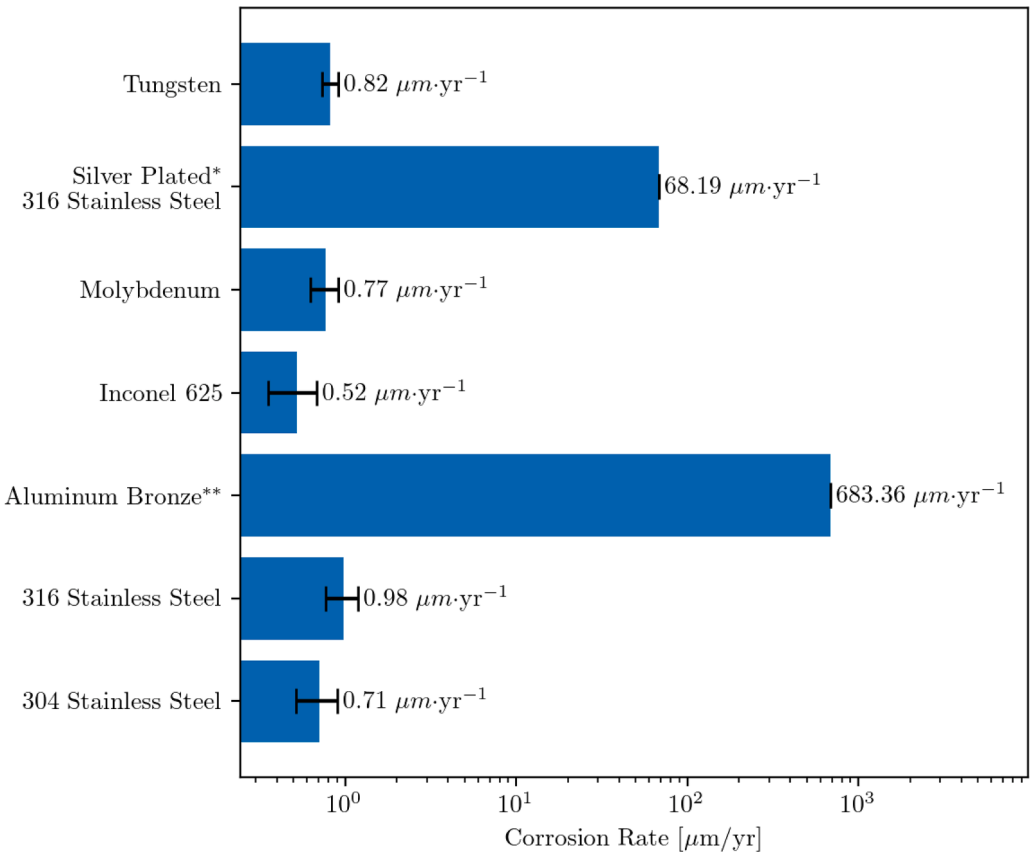

Fig. 11. Comparison of the corrosion rates of all materials tested. The corrosion rate calculated removes the density dependence in mass loss-based rates and is a more direct comparison between materials. *Corrosion rate is likely much greater than reported, due to complete removal of silver layer. **Corrosion rate is likely much greater than reported, due to copper saturation of liquid lithium.

Table 4
Overview of material degradation of all seven materials tested after lithium exposure for 100 h at 300 °C.

Material	Appearance	Surface Structure
Tungsten	- slight discoloration	- no conclusive roughness changes
Molybdenum	- slight discoloration	- no conclusive roughness changes - potential loss of grooves
304 Stainless Steel	- little surface discoloration	- no conclusive roughness changes
316 Stainless Steel	- little surface discoloration	- no conclusive roughness changes
Inconel 625	- little surface discoloration	- no conclusive roughness changes
Silver-plated 316 Stainless Steel	- very dark	- considerably rougher
Aluminum Bronze	- grayish-brown and porous	- considerably rougher

Material	Mass Change	Chemical Changes
Tungsten	- minimal mass loss	- no noticeable changes - lithium-based-deposits on surface
Molybdenum	- minimal mass loss	- no bulk changes - surface deposits of Fe, Li, Na, Mg, O
304 Stainless Steel	- minimal mass loss	- no noticeable changes
316 Stainless Steel	- minimal mass loss	- no noticeable changes
Inconel 625	- very minimal mass loss	- no noticeable changes
Silver-plated 316 Stainless Steel	- large	- total removal of silver
Aluminum Bronze	- very large	- loss of copper

The refractory metals, tungsten and molybdenum, performed well in the lithium environment. Neither material suffered large mass loss during testing. In agreement with literature, the refractory metal corrosion seems to be based on the dissolution of the metal into the lithium solution. The structural materials, 304 stainless steel, 316 stainless steel, and Inconel 625, also performed well during the lithium exposure. Mass loss was minimal and the surfaces remained polished after exposure. Both of these groups of materials seem to be acceptable candidates for use in liquid lithium PFCs environments. On the other hand, the bolt materials, silver-plated 316 stainless steel and aluminum bronze, completely failed under lithium exposure. The silver plating was entirely removed from the plated sample, nullify the benefits of the coating and adding impurities to the lithium. The aluminum bronze samples lost large amounts of mass and were likely only remaining because there was not enough lithium remaining to continue to form reaction products.

Moving forward, additional testing needs to be performed to determine the longevity of these materials in changing environments. A temperature sweep should be conducted to make sure there is not a major change in corrosion rate with temperature, and flowing corrosion testing should be done for lithium PFCs systems. Further investigation is needed to test novel materials or coatings for use as bolts in a liquid lithium environment for fusion reactors elemental transfer, intergranular attack, influence of impurities, and influence of lithium flow are suggested for future investigations.

CRediT authorship contribution statement

Cody D. Moynihan: Conceptualization, Data curation, Formal analysis, Investigation, Software, Validation, Writing – original draft. **Steven Stemmley:** Conceptualization, Data curation, Formal analysis, Investigation, Methodology, Software. **Brady Moore:** Data curation, Investigation, Software, Validation. **Riley Trendler:** Data curation, Formal analysis, Investigation, Software. **Md. Amzad Hossain:** Formal analysis, Investigation, Validation, Visualization, Writing – original draft, Writing – review & editing. **David N. Ruzic:** Conceptualization, Data curation, Formal analysis, Funding acquisition, Investigation, Methodology, Project administration, Resources, Software, Supervision, Validation, Visualization, Writing – original draft, Writing – review & editing.

Declaration of Competing Interest

The authors declare that they have no known competing financial interests or personal relationships that could have appeared to influence the work reported in this paper.

Data availability

The data that support the findings of this study are available within the article based on the request.

Data will be made available on request.

Acknowledgments

This research was financed by Tokamak Energy Ltd. The authors are grateful for the characterization analysis which was carried out in part at the Materials Research Laboratory Central Research Facilities, University of Illinois Urbana-Champaign.

References

[1] A. De Castro, C. Moynihan, S. Stemmley, M. Szott, D Ruzic, Lithium, a path to make fusion energy affordable, Phys Plasmas 28 (2021), 050901.
[2] D.K. Mansfield, H.W. Kugel, R. Maingi, M.G. Bell, R. Bell, R. Kaita, J. Kallman, S. Kaye, B. LeBlanc, D. Mueller, S. Paul, R. Raman, L. Roquemore, S. Sabbagh, H. Schneider, C.H. Skinner, V. Soukhanovskii, J. Timberlake, J. Wilgen, L. Zakharov, Transition to ELM-free improved H-mode by lithium deposition on NSTX graphite divertor surfaces, J. Nuclear Mater. 390-391 (2009) 764–767.
[3] M.A. Jaworski, T.K. Gray, M. Antonelli, J.J. Kim, C.Y. Lau, M.B. Lee, M. J. Neumann, W. Xu, D.N. Ruzic, Thermoelectric magnetohydrodynamic stirring of liquid metals, Phys. Rev. Lett. 104 (9) (2010), 094503. Page.
[4] P. Fiflis, A. Press, W. Xu, D. Andruczyk, D. Curreli, D.N. Ruzic, Wetting properties of liquid lithium on select fusion relevant surfaces, Fusion Eng. Design 89 (12) (2014) 2827–2832. Page.
[5] Michael Christenson, Dario Panici, Cody D Moynihan, John Wendeborn, Jacob Anderson, David N Ruzic, A study on hydrogen absorption and dissolution in liquid lithium, Nuclear Fusion 59 (2) (2019), 026011. Number.
[6] Michael Christenson, Cody D. Moynihan, David N. Ruzic, A distillation column for hydrogen isotope removal from liquid lithium, Fusion Eng. Design 135 (2018) 81–87.
[7] R. Bamber, D. Iglesias, O. Asunta, et al., The ST40 IVC1 divertor project: procurement and installation in times of COVID-19, En, Fusion Eng. Des. 168 (112378) (2021) 112 378.
[8] T. Hirai, F. Escourbiac, S. Carpentier-Chouchana, et al., ITER tungsten divertor design development and qualification program, En, Fusion Eng. Des. 88 (9–10) (2013) 1798–1801.
[9] L. Cao, Z. Zhou, D. Yao, EAST full tungsten divertor design, En, J. Fusion Energy 34 (6) (Dec. 2015) 1451–1456.
[10] W.R. Wampler, D.L. Rudakov, J.G. Watkins, A.G. McLean, E.A. Unterberg, P. C. Stangeby, Measurements of tungsten migration in the DIII-D divertor, Phys. Scr. T170 (2017) 014 041.
[11] R.A. Causet, T.J. Venhaus, The use of tungsten in fusion reactors: a review of the hydrogen retention and migration properties, en, Phys. Scr. T94 (1) (2001) 9.
[12] G.F. Matthews, B. Bazylev, A. Baron-Wiechec, et al., Melt damage to the JET ITER-like wall and divertor, Phys. Scr. T167 (2016) 014 070.
[13] P. Fiflis, D. Curreli, D.N. Ruzic, Direct time-resolved observation of tungsten nanostructured growth due to helium plasma exposure, Nuclear Fusion 55 (3) (2015) 033 020.
[14] S. Kajita, N. Yoshida, N. Ohno, Tungsten fuzz: deposition effects and influence to fusion devices, en, Nucl. Mater. Energy 25 (100828) (2020) 100 828.
[15] J.A.R. Wright, A review of late-stage tungsten fuzz growth, en, Tungsten 4 (3) (2022) 184–193.
[16] A. Khodak, R. Maingi, Plasma facing components with capillary porous system and liquid metal coolant flow, Phys. Plasmas 29 (7) (2022) 072 505.
[17] J.E. Menard, T. Brown, M.Boyer L.El-Guebaly, J. Canik, B. Colling, R. Raman, Z. Wang, Y. Zhai, P. Buxton, B. Covele, C. D'Angelo, A. Davis, S. Gerhardt, M. Gryaznevich, M. Harb, T.C. Hender, .. Kaye, D. Kingham, M. Kotschenreuther, S. Mahajan, R. Maingi, E. Marriott, E.T. Meier, L. Mynsberge, C. Neumeyer, M. Ono, J.-K. Park, S.A. Sabbagh, V. Soukhanovskii, P. Valanju, R. Woolley, Fusion nuclear science facilities and pilot plants based on the spherical tokamak, Nuclear Fusion 56 (2016), 106023.
[18] R.J. Goldston, R. Myers, J. Schwartz, The lithium vapor box divertor, Phys. Scr. T167 (2016) 014 017.
[19] D.N. Ruzic, W. Xu, D. Andruczyk, M.A. Jaworski, Lithium–metal infused trenches (LiMIT) for heat removal in fusion devices, Nuclear Fusion 51 (10) (2011) 102 002.
[20] J.S. Hu, G.Z. Zuo, R. Maingi, et al., Experiments of continuously and stably flowing lithium limiter in EAST towards a solution for the power exhaust of future fusion devices, en, Nuclear Mater. Energy 18 (2019) 99–104.
[21] F.S. Nitti, A. Ibarra, M. Ida, et al., The design status of the liquid lithium target facility of IFMIF at the end of the engineering design activities, en, Fusion Eng. Des. 100 (2015) 425–430.
[22] E. Kolemen, M. Hvasta, R. Majeski, R. Maingi, A. Brooks, T. Kozub, Design of the flowing LIquid torus (FLIT), en, Nucl. Mater. Energy 19 (2019) 524–530.
[23] D.R. Lide, CRC Handbook of Chemistry and Physics, 85, CRC press, 2004.
[24] M. Christenson, C. Moynihan, D.N. Ruzic, A distillation column for hydrogen isotope removal from liquid lithium, Fusion Eng. Des. 135 (2018) 81–87.
[25] T.F. Fuerst, C.N. Taylor, P.W. Humrickhouse, The source permeator system and tritium transport in the TEX PbLi loop, en, Fusion Sci. Technol. 79 (1) (2023) 77–94.
[26] A. Khodak, F. Yang, H.A. Stone, Free-surface liquid lithium flow modeling and stability analysis for fusion applications," en, J. Fusion Energy 39 (6) (2020) 455–461.
[27] M. Szott, S. Stemmley, C. Moynihan, A. de Castro, D.N. Ruzic, Structured large-pore foams im- prove thermal performance of LiMIT-style liquid lithium PFC, Nuclear Fusion 62 (1) (2022) 016 018.
[28] P. Fiflis, M. Christenson, M. Szott, K. Kalathiparambil, D.N. Ruzic, Free surface stability of liquid metal plasma facing components, Nuclear Fusion 56 (10) (2016) 106 020.
[29] X. Meng, G. Zuo, Z. Sun, et al., Compatibility of molybdenum, tungsten, and 304 stainless steel in static liquid lithium under high vacuum, Plasma Phys. Reports 44 (7) (2018) 671–677.

[30] G. DeVries, The corrosion of metals by molten lithium. Corrosion By Liquid Metals, Springer US, 1970, pp. 251–269.
[31] O.K. Chopra, D.L. Smith, P.F. Tortorelli, J.H. DeVan, D.K. Sze, Liquid-metal corrosion, Fusion Technol. 8 (2 pt 1) (1985) 1956–1969, issn: 07481896.
[32] V. Coen, H. Kolbe, L. Orecchia, and T. Sasaki, "Compatibility of high Ni, Fe-Cr alloys in Li containing traces of LiH", pp. 121–130, 1982.
[33] E. Ruedl, V. Coen, T. Sasaki, H. Kolbe, Influence of lithium on the structural stability of two austenitic stainless steels of the type 316 and 18 mn-10 Cr,. Material Behavior and Physical Chemistry in Liquid Metal Systems, Springer, US, 1982, pp. 97–104.
[34] X.C. Meng, C. Xu, G.Z. Zuo, Corrosion characteristics of copper in static liquid lithium under high vacuum, J. Nuclear Mater. 513 (2019) 282–292.
[35] P. He, Z. Zhang, W. Xia, Compatibility between high-flux helium plasma irradiated molyb- denum and liquid lithium, J. Nuclear Mater. 509 (2018) 736–741.
[36] X. Meng, L. Li, C. Li, Corrosion characteristics of mo and tzm alloy for plasma facing compo- nents in molten lithium at 623 k, Corros Sci 200 (2022) 110 202.
[37] D. Zhang, X. Meng, G. Zuo, Study of the corrosion characteristics of 304 and 316l stainless steel in the static liquid lithium, J. Nuclear Mater. 553 (2021) 153 032.
[38] C. Xu, X. Meng, X. Sun, Atomic scale analysis of the corrosion characteristics of Cu-Li solid- liquid interfaces, J. Alloys Compd. 763 (2018) 1–10.
[39] J.A.D. Mastry, Corrosion studies of tungsten, molybdenum, and rhenium in lithium, Nuclear Appl. 3 (2) (1967) 127–134.
[40] X. Meng, G. Zuo, W. Xu, Effect of temperature on the corrosion behaviors of 304 stainless steel in static liquid lithium, Fusion Eng. Design 128 (2018) 75–81.